Electronic Supplementary Material (ESI) for Photochemical & Photobiological Sciences.
This journal is © The Royal Society of Chemistry and Owner Societies 2018

Supporting Information

A multiple target chemosensor for the sequential fluorescence detection of Zn^{2+} and S^{2-} and the colorimetric detection of $Fe^{3+/2+}$ in aqueous media and living cells

Jin Yeong Yun,[a] Ju Byeong Chae,[a] Mingeun Kim,[b,c] Mi Hee Lim,[c] Cheal Kim[a]*

[a]*Depart. of Fine Chem., SNUT (Seoul National Univ. of Sci. and Tech.), Seoul 01188, Republic of Korea. Fax: +82-2-983-9149; Tel: +82-2-970-6680; E-mail: chealkim@seoultech.ac.kr*

[b]*Department of Chemistry, Ulsan National Institute of Science and Technology (UNIST), Ulsan 44919, Republic of Korea*

[c]*Department of Chemistry, Korea Advanced Institute of Science and Technology (KAIST), Daejeon 34141, Republic of Korea*

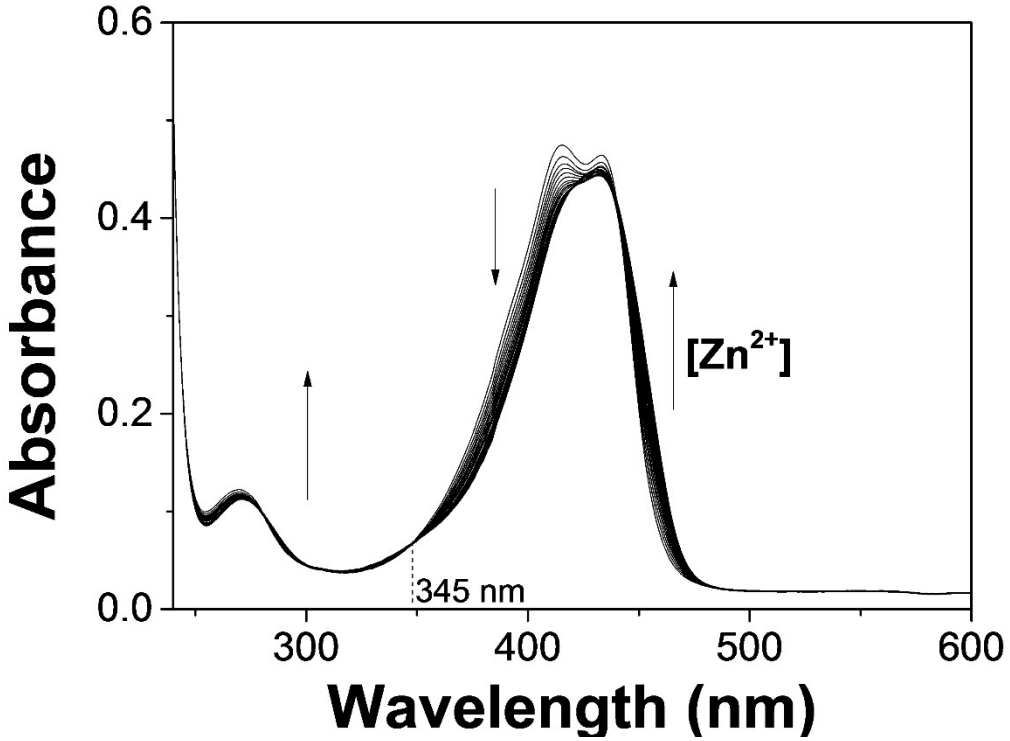

Fig. S1 UV-vis absorption spectral changes of **DHIC** (10 μM) in the presence of different concentrations of Zn^{2+} (from 0 to 14 equiv).

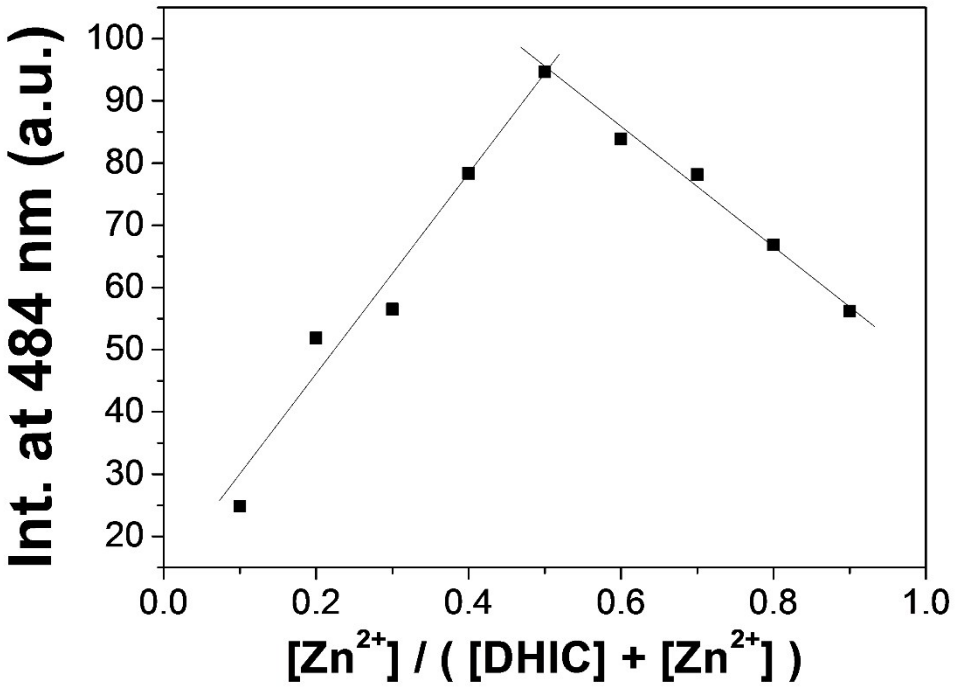

Fig. S2 Job plot for the binding of **DHIC** with Zn^{2+}. Fluorescence intensity at 484 nm was plotted as a function of the molar ratio of $[Zn^{2+}]$ / ([**DHIC**] + $[Zn^{2+}]$). The total concentrations of Zn^{2+} with **DHIC** were 40 μM.

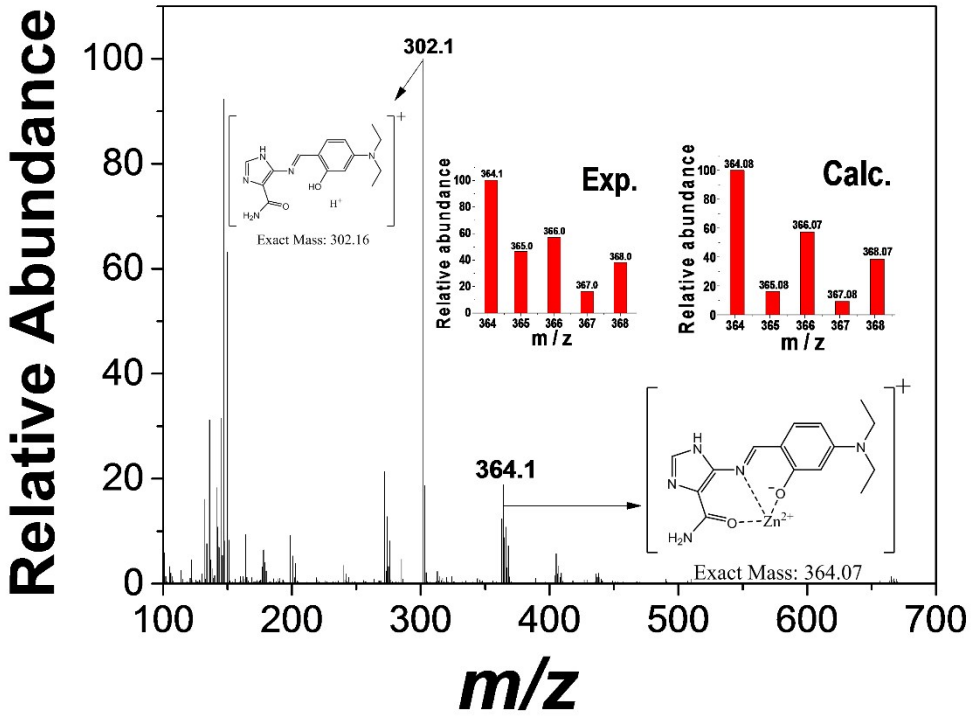

Fig. S3 Positive-ion electrospray ionization mass spectrum of **DHIC** (100 μM) upon addition of $Zn(NO_3)_2$ (1 equiv).

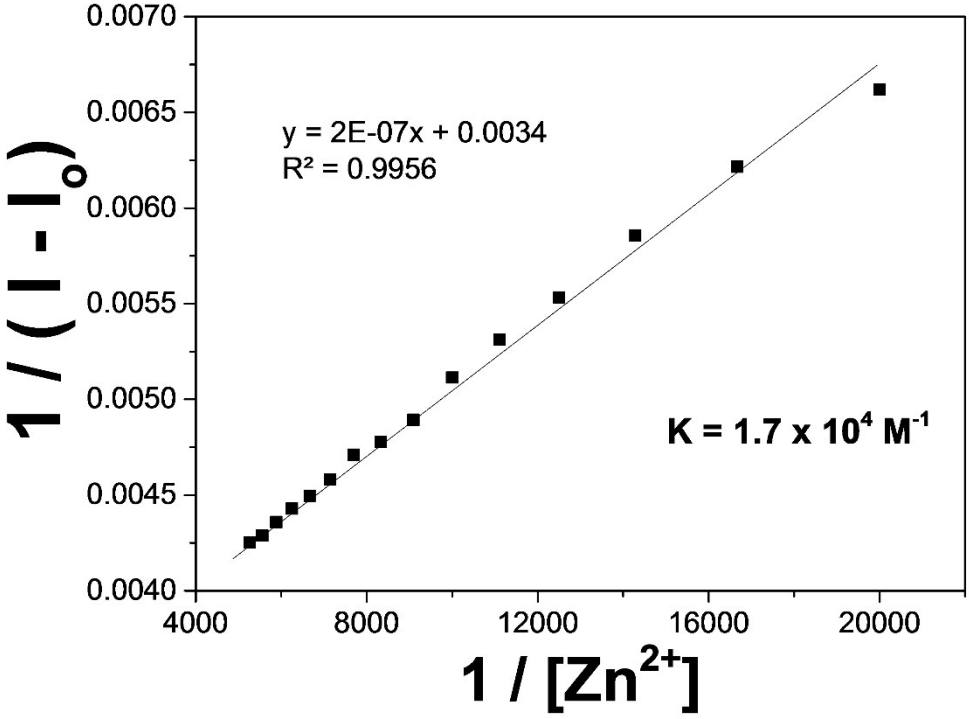

Fig. S4 Benesi-Hildebrand plot (fluorescence intensity at 484 nm) of **DHIC** (10 μM) based on fluorescence titration, assuming 1:1 ratio for association between **DHIC** and Zn^{2+}.

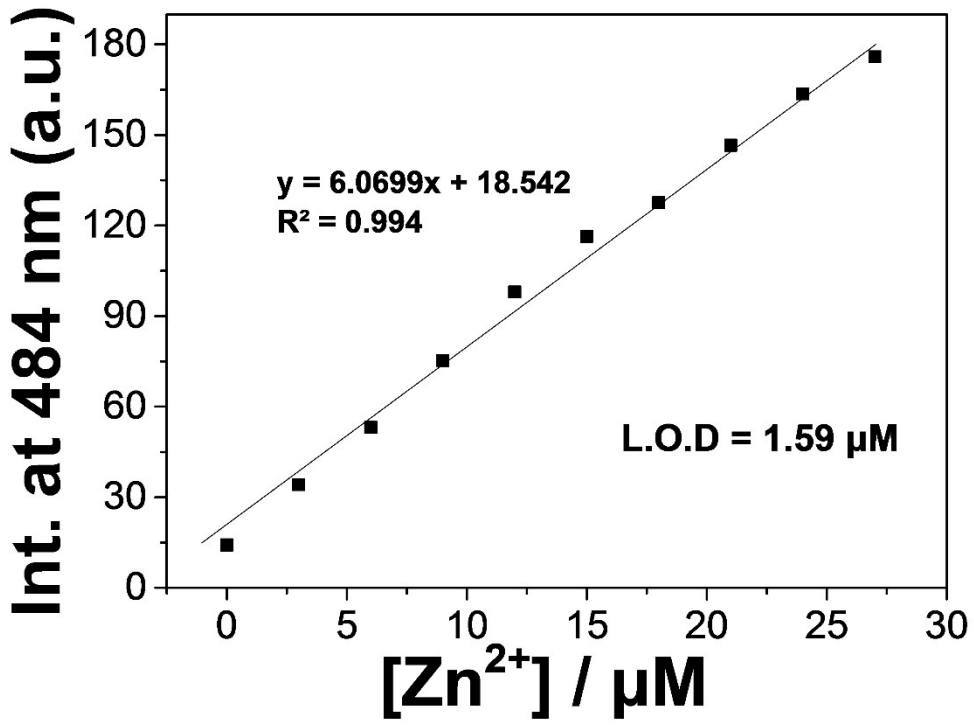

Fig. S5 Limit of detection based on change in the ratio (fluorescence intensity at 484 nm) of **DHIC** (10 µM) with Zn^{2+}.

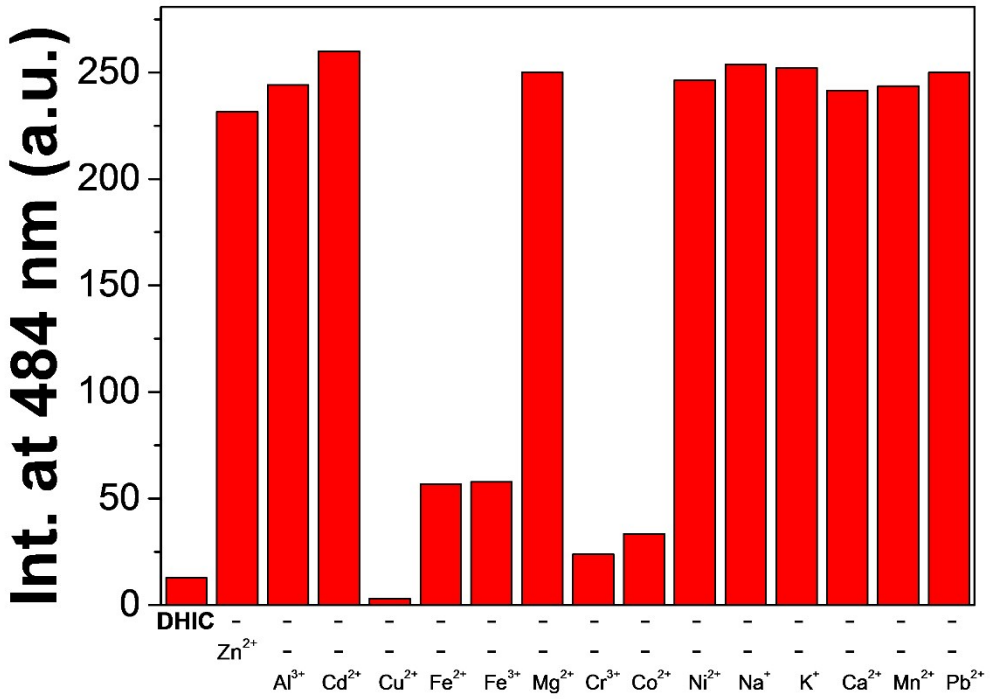

Fig. S6 Competitive experiment of **DHIC** (10 μM) toward Zn^{2+} (21 equiv) in the presence of other metal ions (21 equiv) with an excitation of 420 nm.

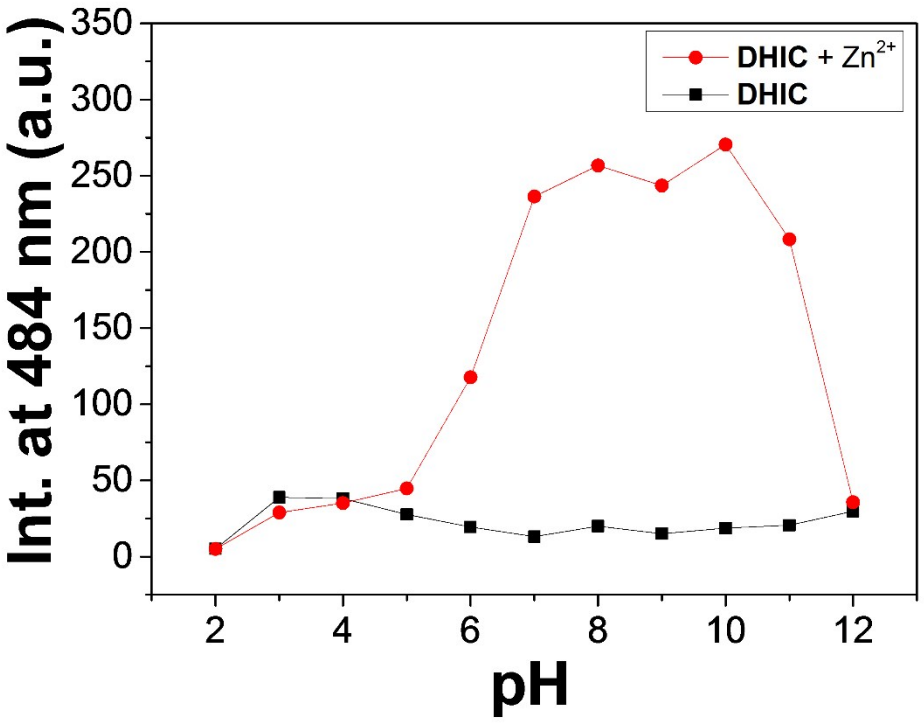

Fig. S7 Fluorescence intensities (at 484 nm) of **DHIC** (10 μM) and of **DHIC**-Zn^{2+} complex, respectively, at different pH values (2-12).

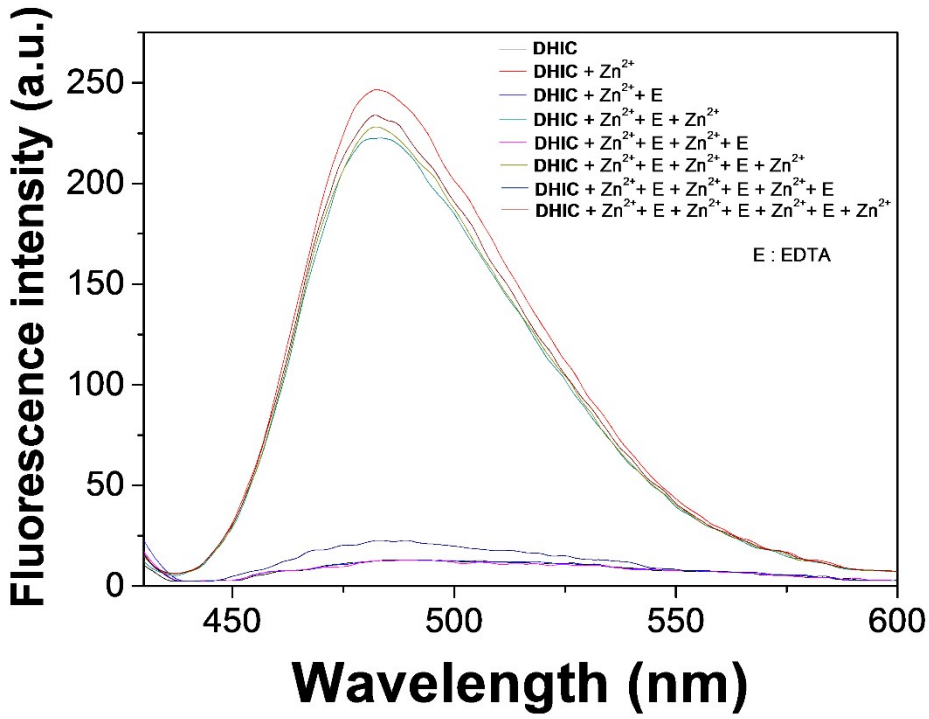

Fig. S8 Fluorescence intensity changes of **DHIC** (10 μM) after the sequential addition of Zn^{2+} and EDTA.

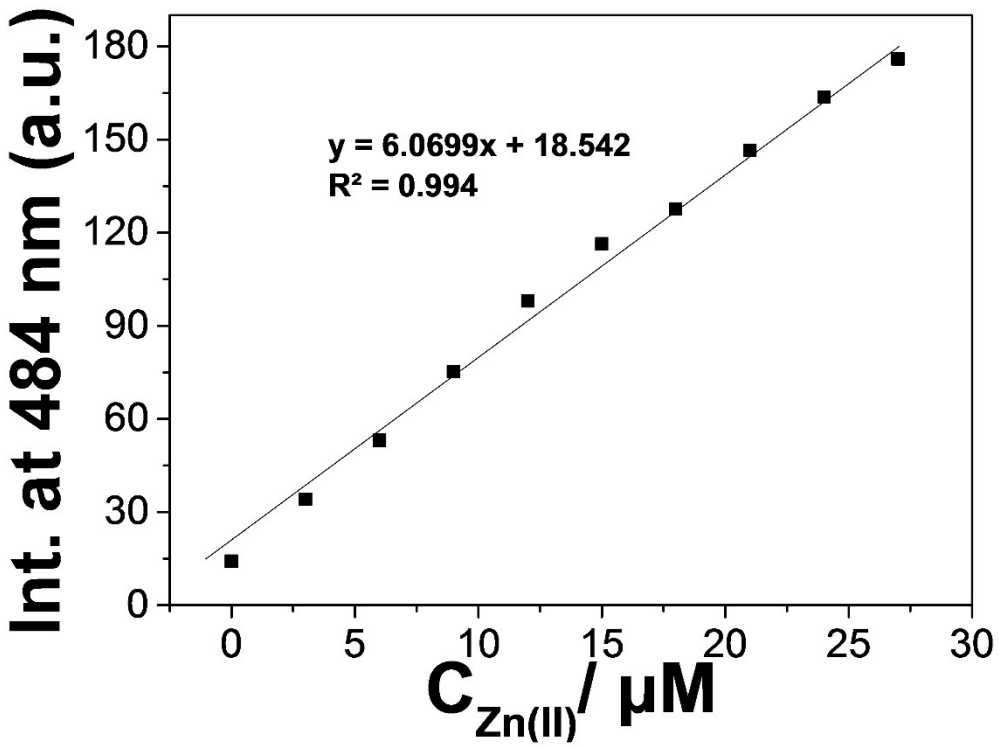

Fig. S9 Fluorescence intensity (at 484 nm) of **DHIC** as a function of Zn^{2+} concentration ([**DHIC**] = 10 μM and [Zn^{2+}] = 0.0–27.0 μM).

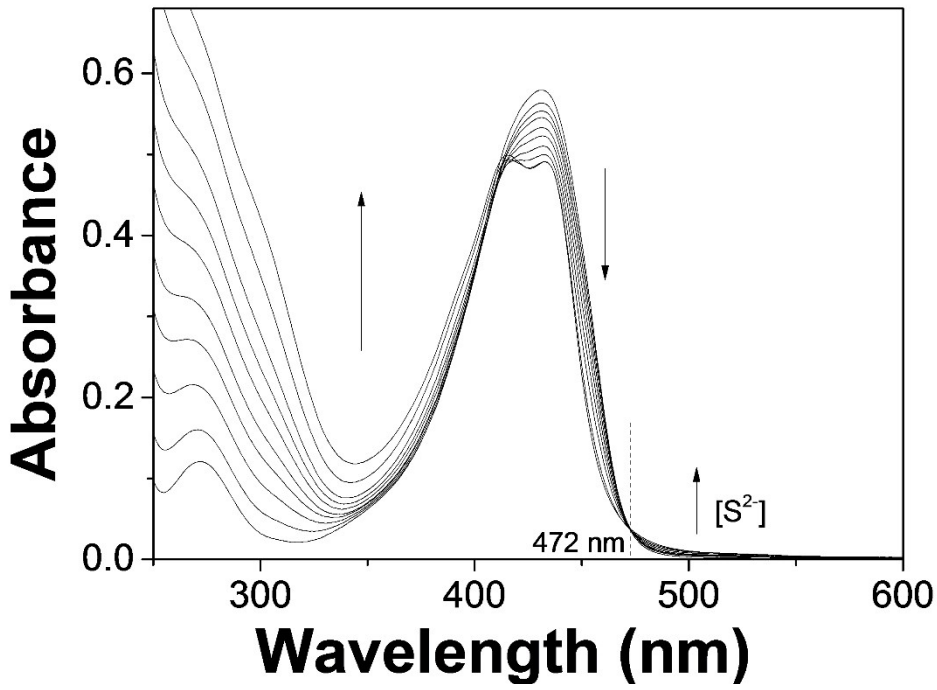

Fig. S10 UV-vis absorption spectral changes of **DHIC**-Zn^{2+} (10 μM) in the presence of different concentrations of S^{2-} (from 0 to 27 equiv).

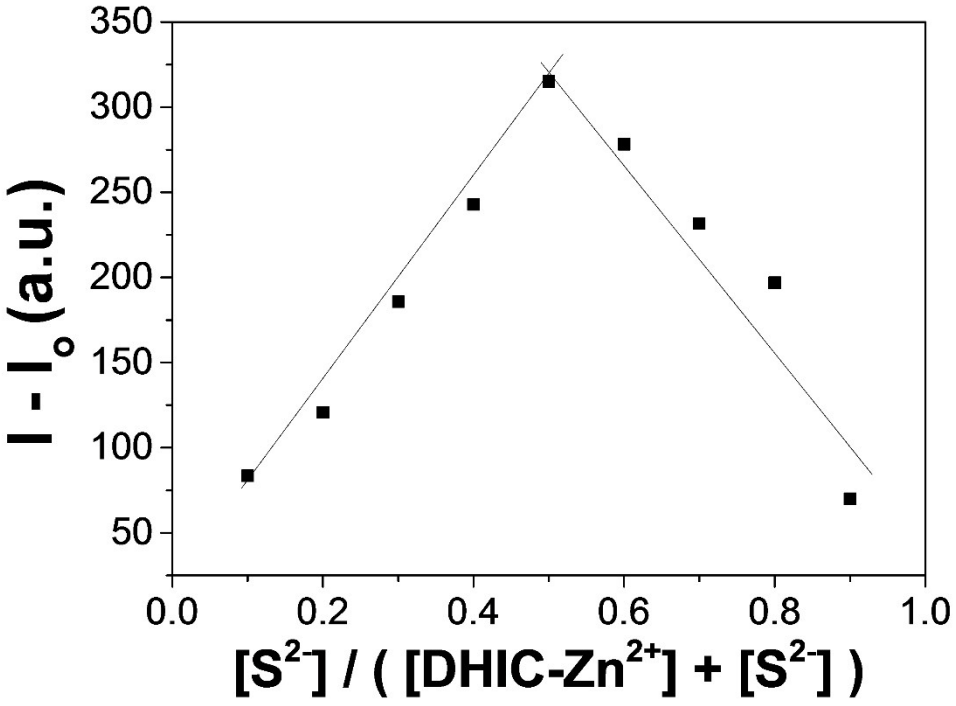

Fig. S11 Job plot for the binding of **DHIC**-Zn^{2+} with S^{2-}. Difference of fluorescence intensity at 484 nm was plotted as a function of the molar ratio of $[S^{2-}]$ / ([**DHIC**-Zn^{2+}] + $[S^{2-}]$). The total concentrations of S^{2-} with **DHIC**-Zn^{2+} complex were 200 μM.

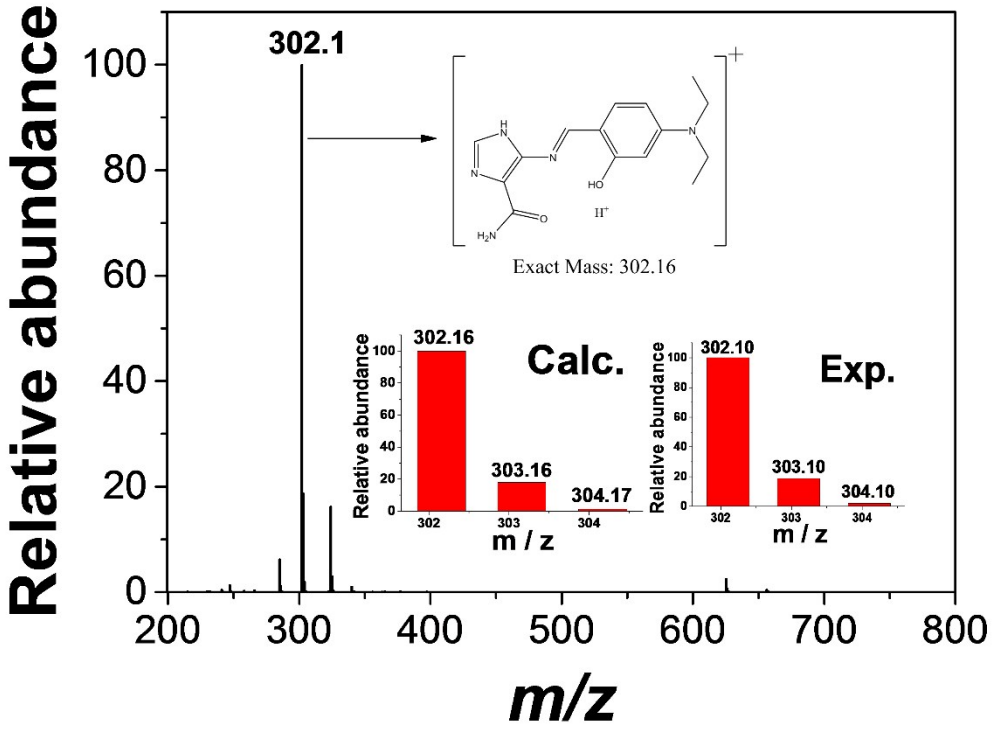

Fig. S12 Positive-ion electrospray ionization mass spectrum of **DHIC**-Zn^{2+} (100 μM) upon addition of Na_2S (1 equiv).

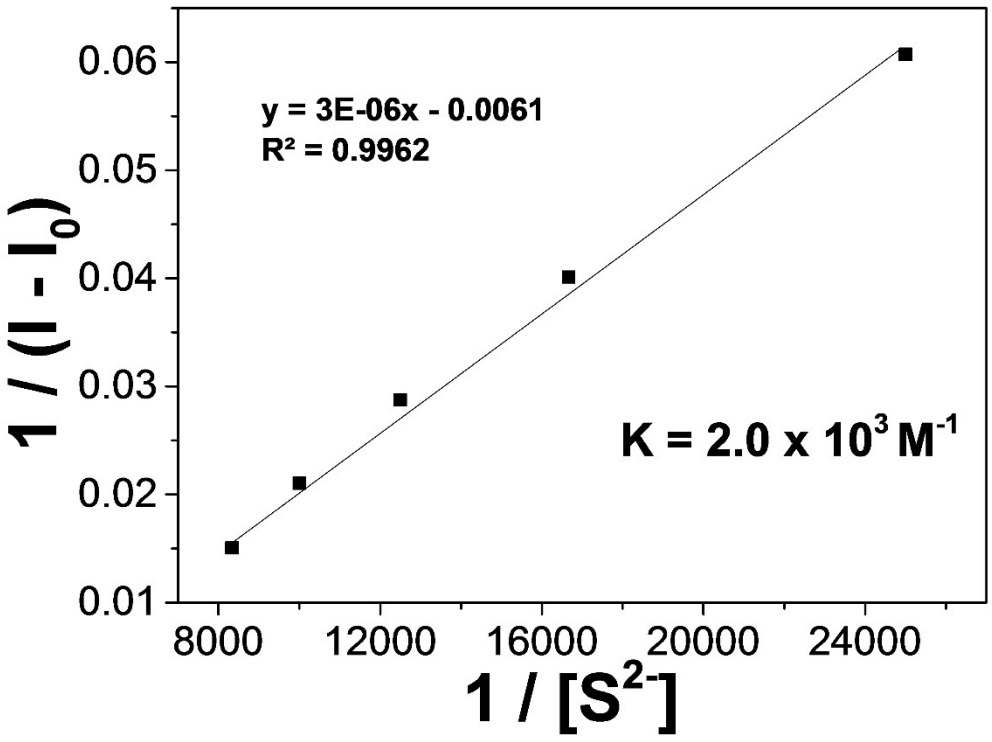

Fig. S13 Benesi-Hildebrand plot (fluorescence intensity at 484 nm) of **DHIC**-Zn^{2+} (10 μM) based on fluorescence titration, assuming 1:1 ratio for association between **DHIC**-Zn^{2+} and S^{2-}.

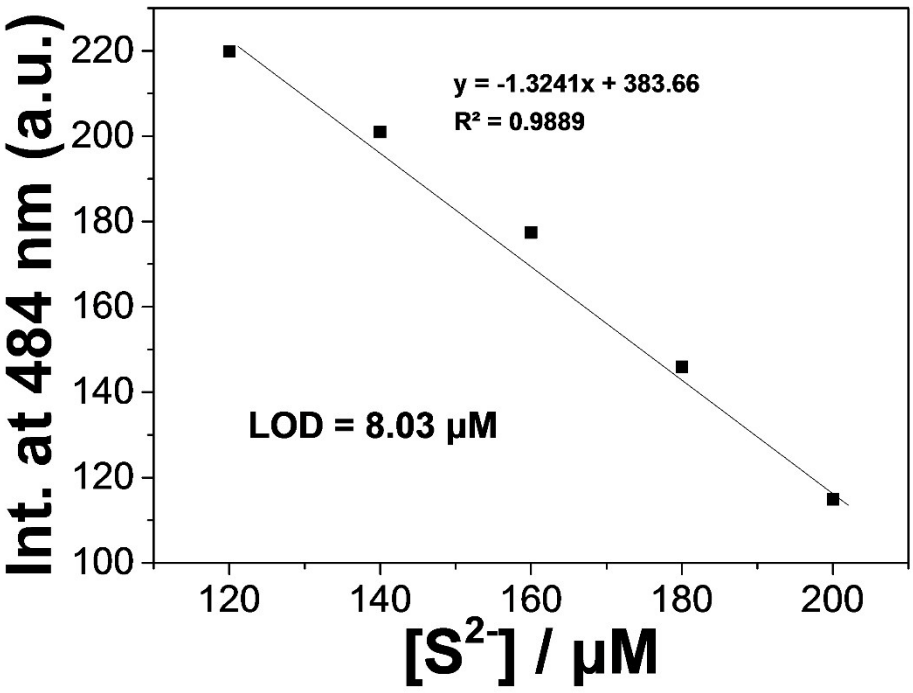

Fig. S14 Limit of detection based on change in the ratio (fluorescence intensity at 484 nm) of **DHIC**-Zn^{2+} (10 µM) with S^{2-}.

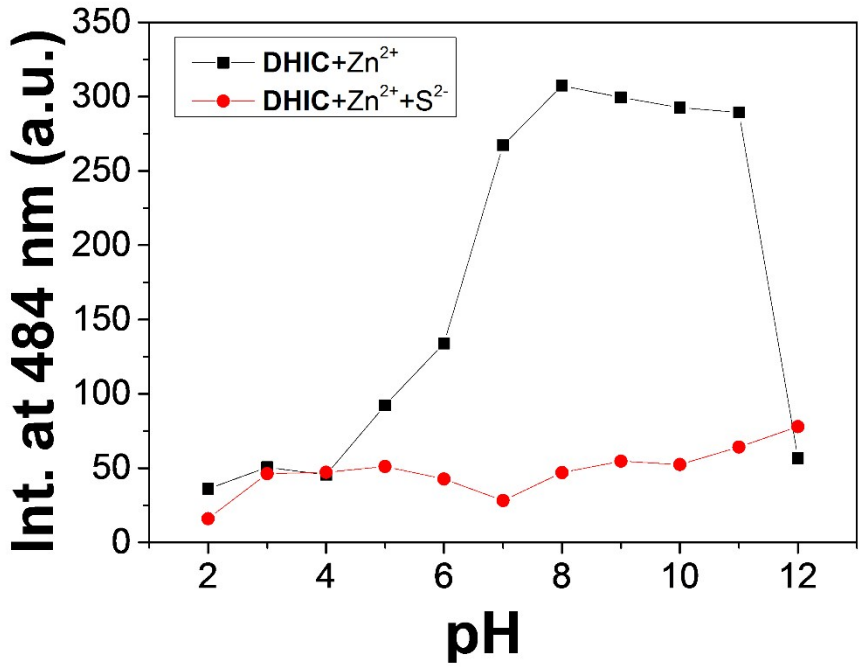

Fig. S15 Fluorescence intensities (at 484 nm) of **DHIC** -Zn^{2+} (10 μM) and **DHIC**-Zn^{2+} + S^{2-} , respectively, at different pH values (2-12).

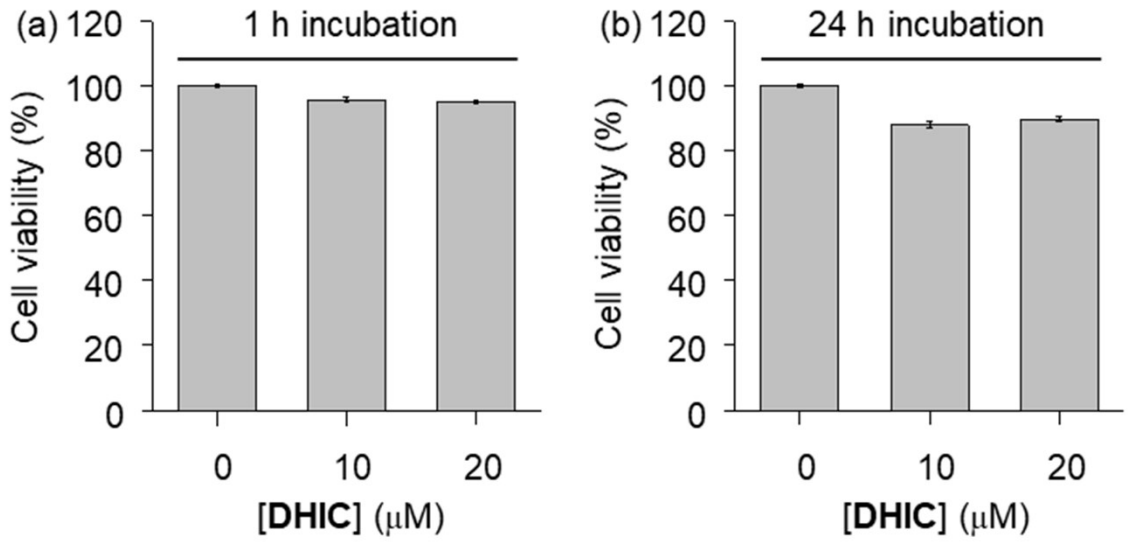

Fig. S16 Cytotoxicity of **DHIC**. **DHIC** (10 and 20 μM; 1% v/v DMSO) was treated to HeLa cells. Cell viability (%) was determined by the MTT assay [MTT = 3-(4,5-dimethylthiazol-2-yl)-2,5-diphenyltetrazolium bromide] in comparison to that of cells treated with DMSO only (1% v/v). Error bars represent the standard error from three independent experiments.

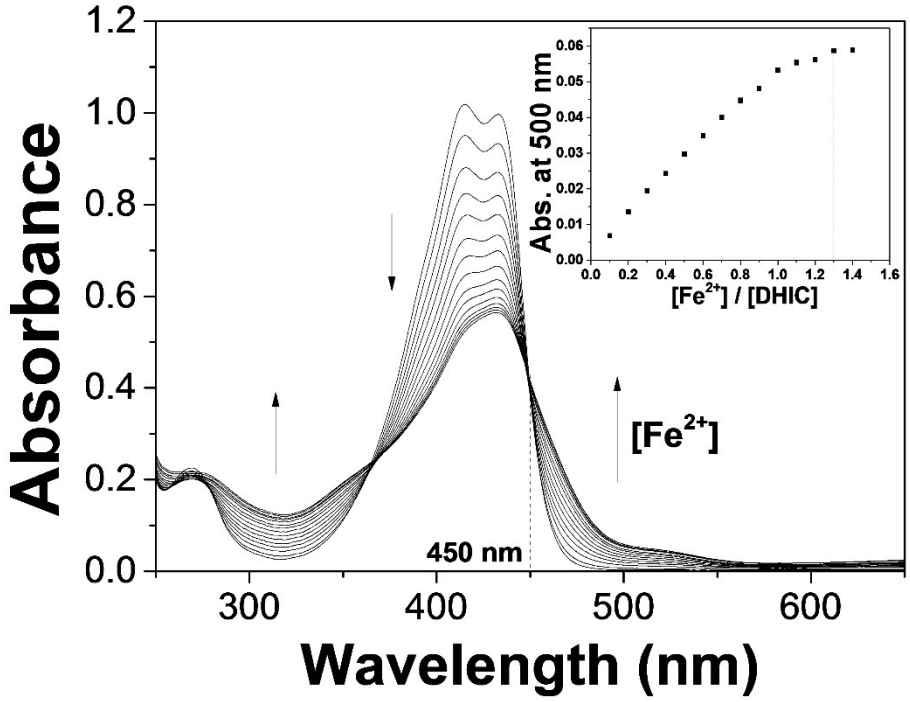

Fig. S17 UV-vis absorption spectral changes of **DHIC** (20 μM) in the presence of different concentrations of Fe^{2+} (from 0 to 1.4 equiv). Inset: Absorbance at 500 nm versus the number of equiv of Fe^{2+} added.

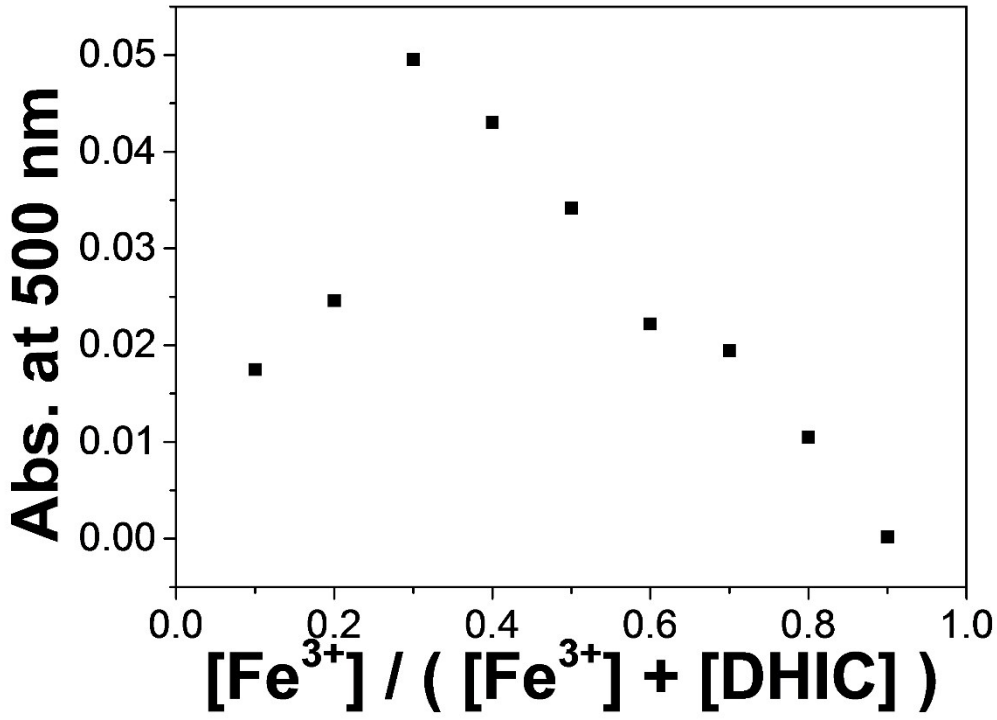

Fig. S18 Job plot for the binding of **DHIC** with Fe^{3+}. UV-vis absorption at 500 nm was plotted as a function of the molar ratio of $[Fe^{3+}]$ / ([**DHIC**] + $[Fe^{3+}]$). The total concentrations of Fe^{3+} with **DHIC** were 20 μM.

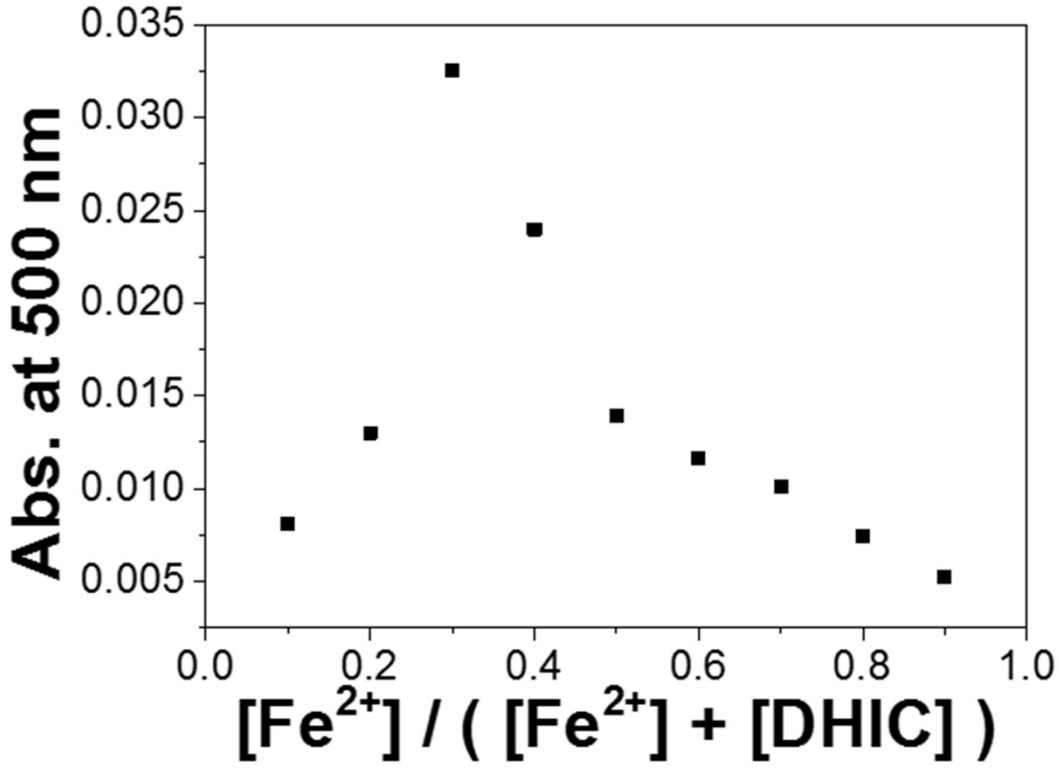

Fig. S19 Job plot for the binding of **DHIC** with Fe^{2+}. UV-vis absorption at 500 nm was plotted as a function of the molar ratio of $[Fe^{2+}]$ / ([**DHIC**] + $[Fe^{2+}]$). The total concentrations of Fe^{2+} with **DHIC** were 20 μM.

(a)

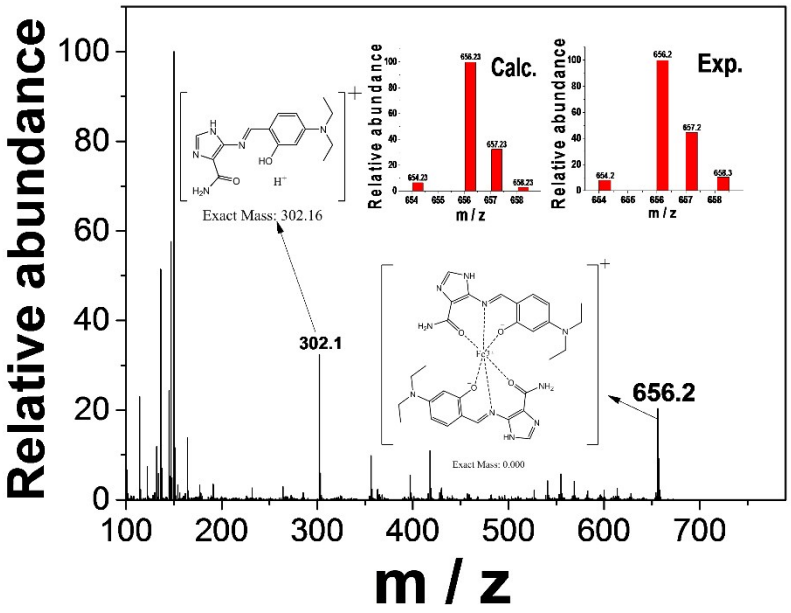

(b)

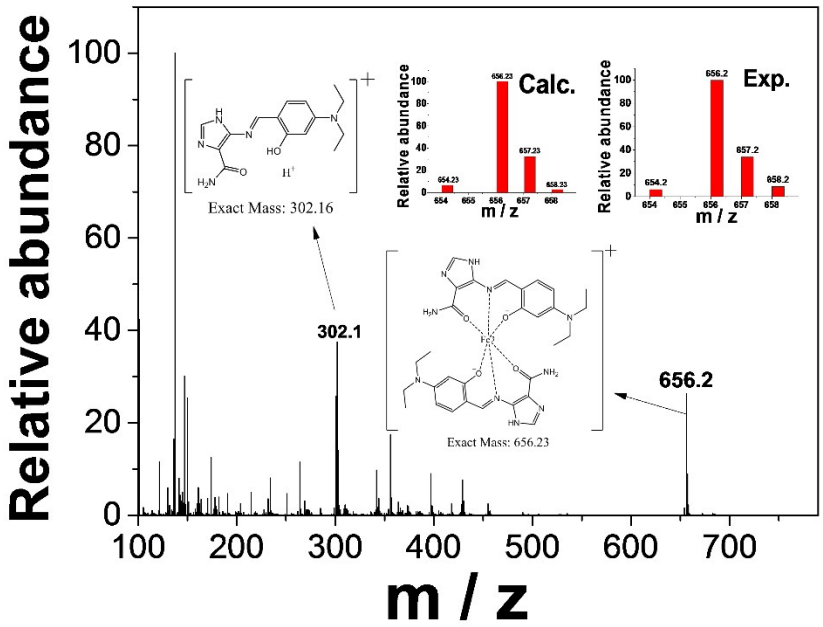

Fig. S20 (a) Positive-ion electrospray ionization mass spectrum of **DHIC** (100 μM) upon addition of $Fe(NO_3)_3$ (1 equiv). (b) Positive-ion electrospray ionization mass spectrum of **DHIC** (100 μM) upon addition of $Fe(ClO_4)_2$ (1 equiv).

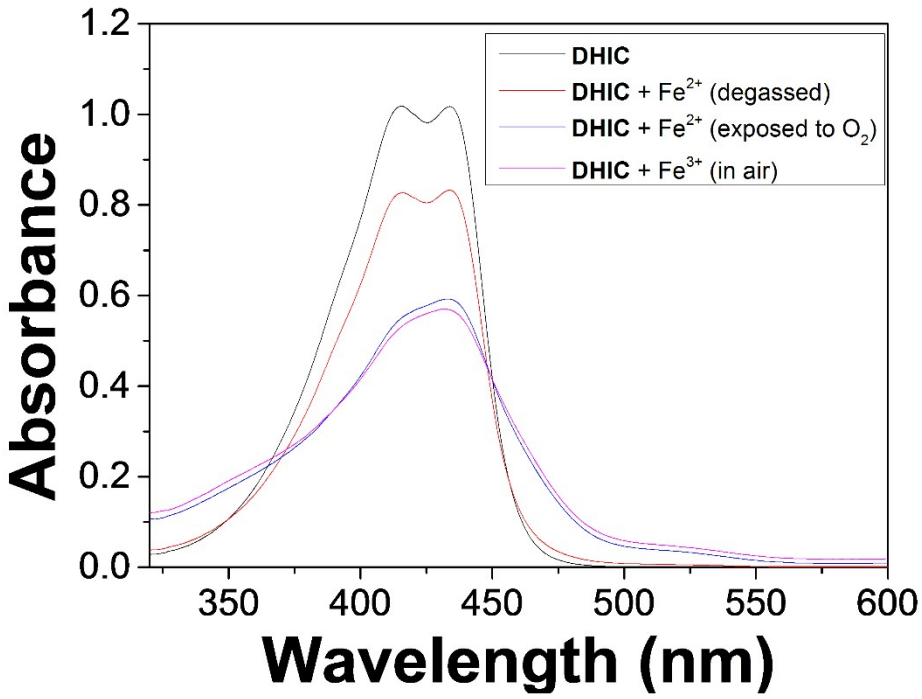

Fig. S21 Absorption spectra of **DHIC** (20 μM) with Fe^{2+} under the degassed and aerobic conditions, and **DHIC** with Fe^{3+} under aerobic conditions.

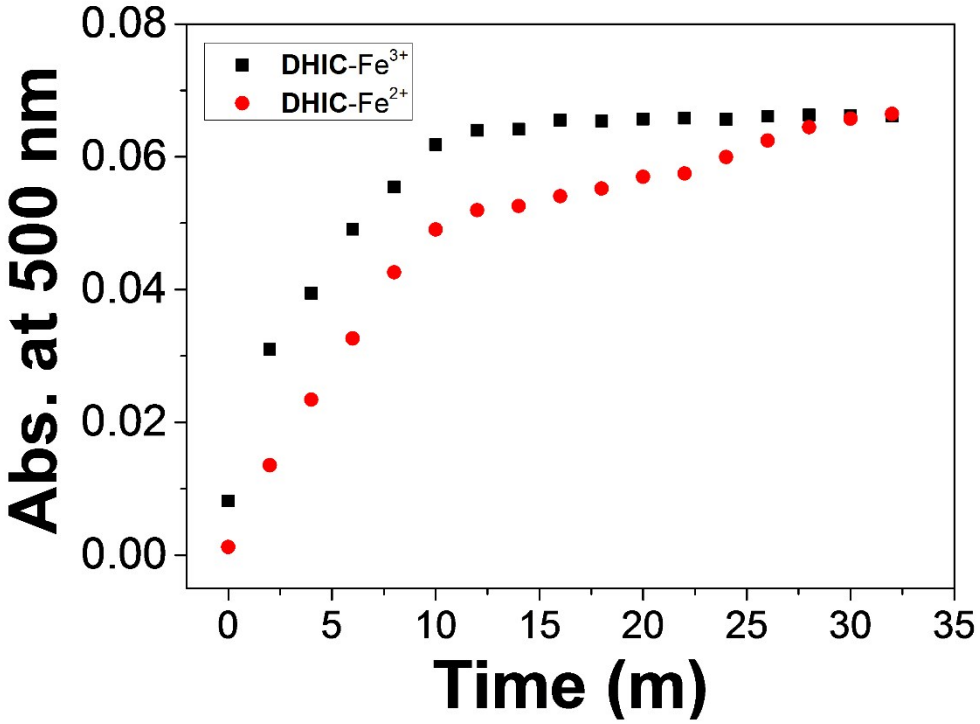

Fig. S22 Formation rates (at 500 nm) of Fe^{3+}-2·**DHIC** complex obtained from the reactions of **DHIC** (20 μM) with $Fe^{3+/2+}$ (1.4 equiv).

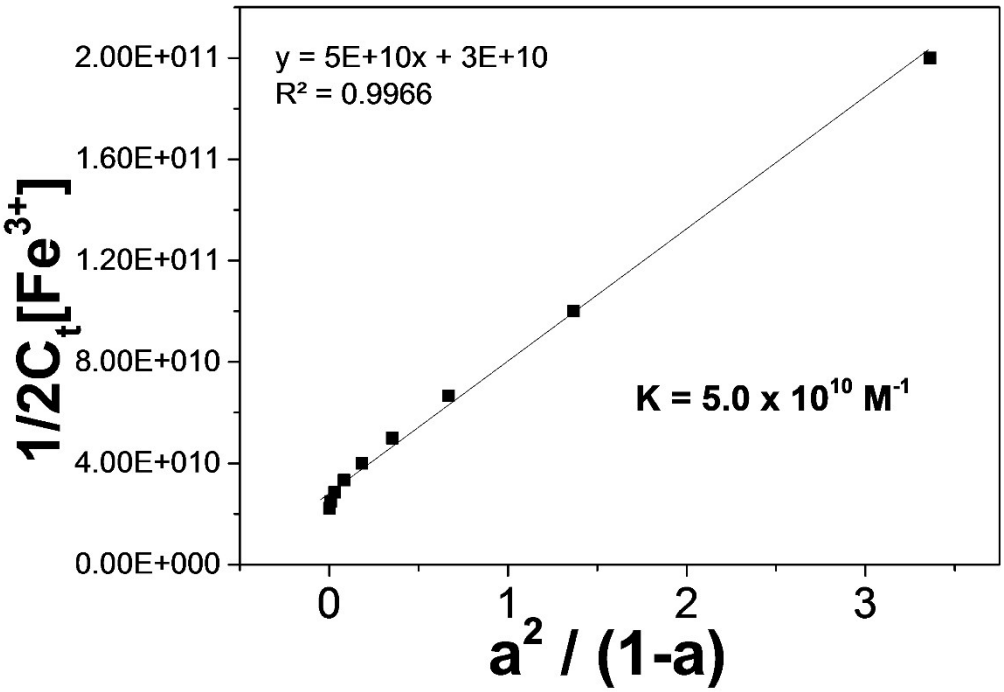

Fig. S23 Li's equation plot plot of Fe^{3+}-2·**DHIC** (20 μM) based on UV-vis titration, assuming 2:1 ratio for association between **DHIC** and Fe^{3+}.

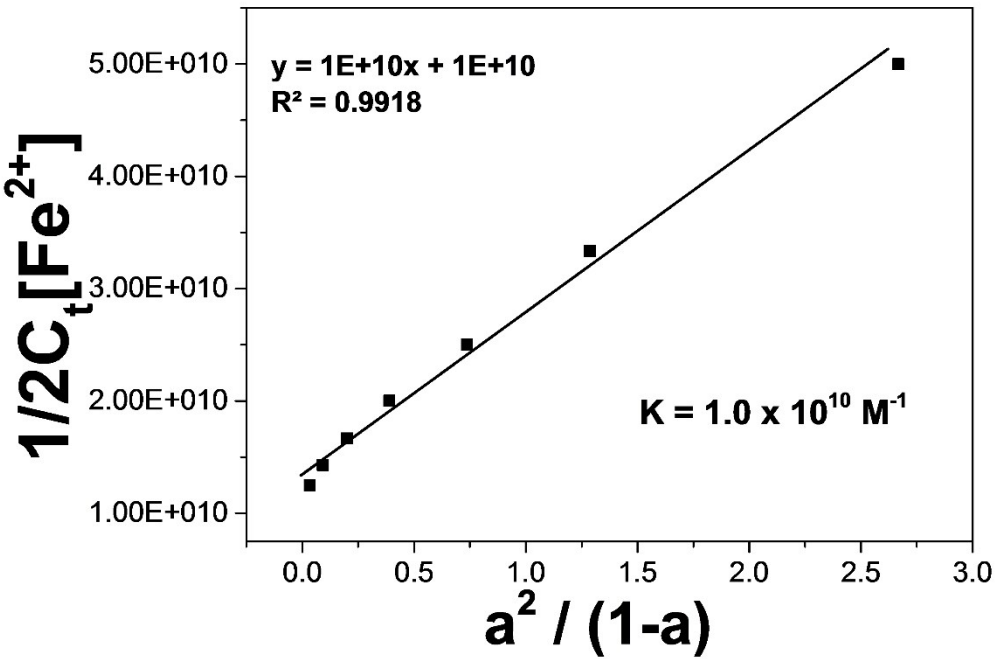

Fig. S24 Li's equation plot of Fe^{2+}-2·**DHIC** (20 μM) based on UV-vis titration, assuming 2:1 ratio for association between **DHIC** and Fe^{2+}.

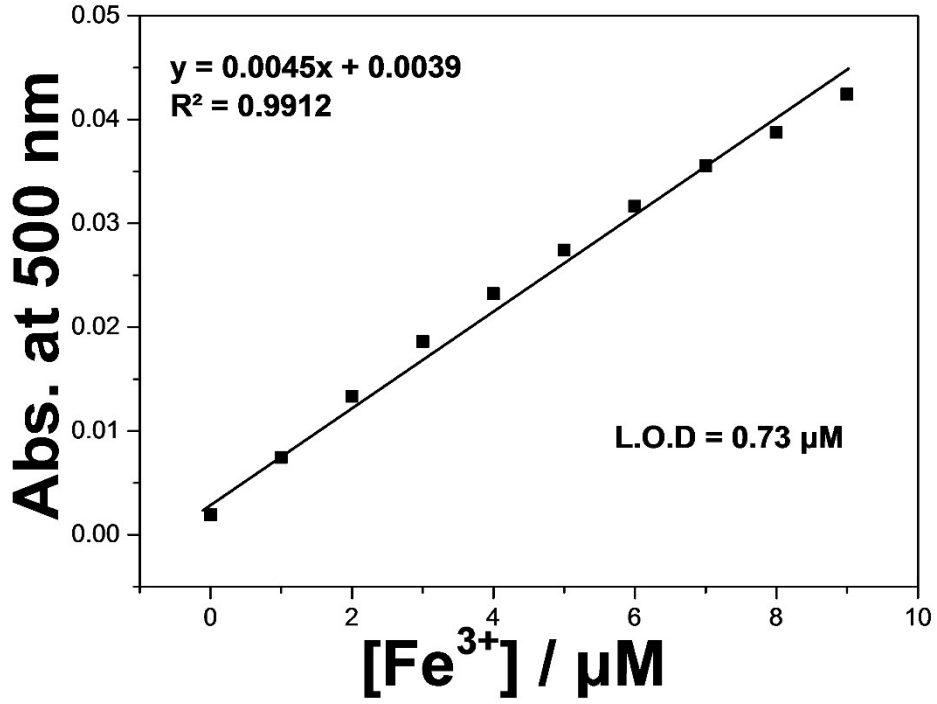

Fig. S25 Limit of detection based on change in the ratio of **DHIC** (20 µM) with Fe^{3+}.

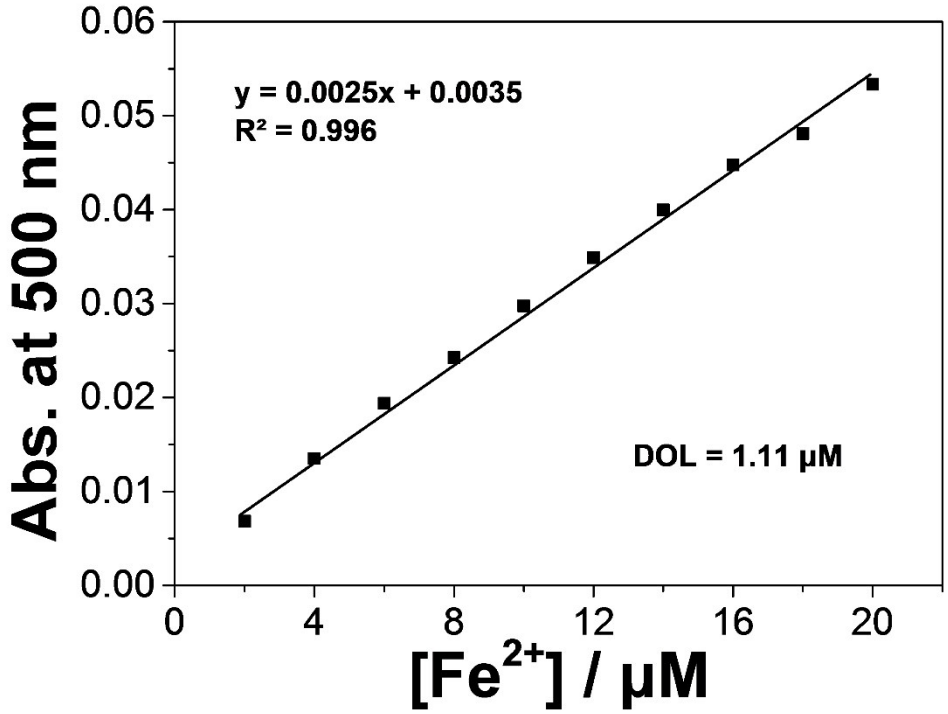

Fig. S26 Limit of detection based on change in the ratio of **DHIC** (20 µM) with Fe^{2+}.

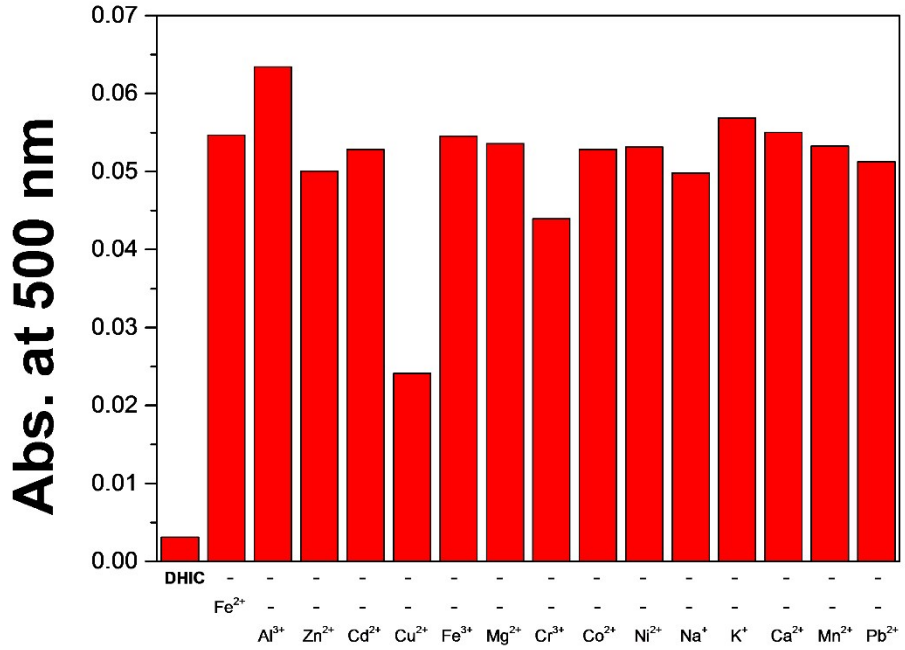

Fig. S27 UV-vis competitive experiment of **DHIC** (20 μM) toward Fe^{2+} in the presence of other metal ions.

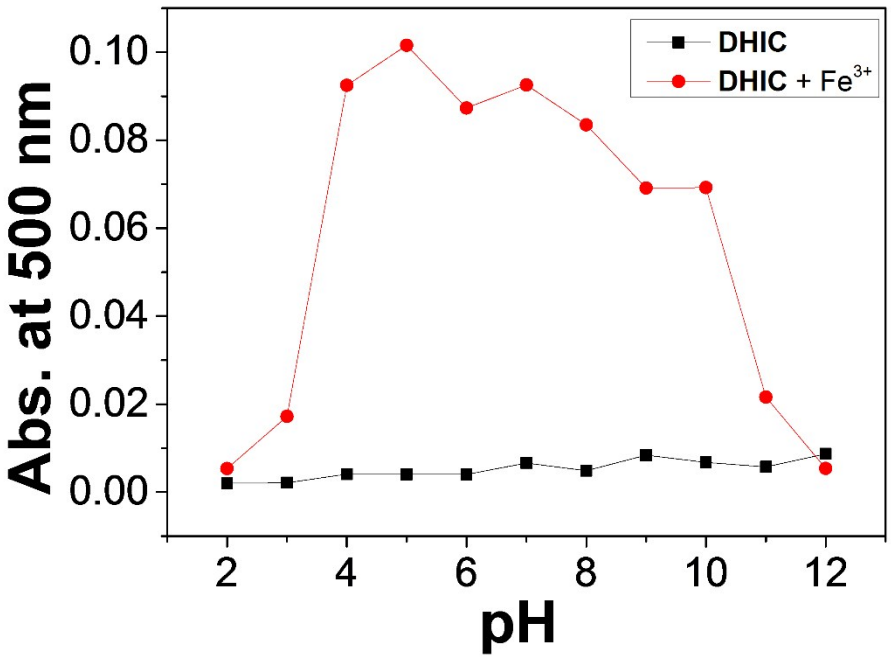

Fig. S28 UV-vis absorption intensity (at 500 nm) of **DHIC** (20 μM) and Fe^{3+}-2·**DHIC**, respectively, at different pH values (2-12).

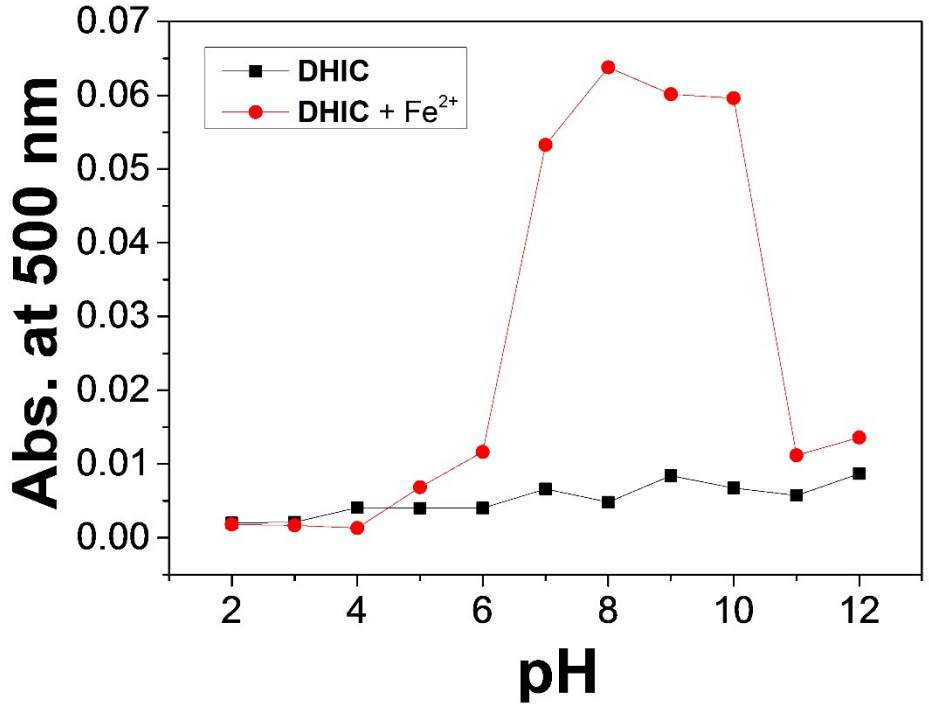

Fig. S29 UV-vis absorption intensity (at 500 nm) of **DHIC** (20 μM) and Fe^{2+}-2·**DHIC**, respectively, at different pH values (2-12).

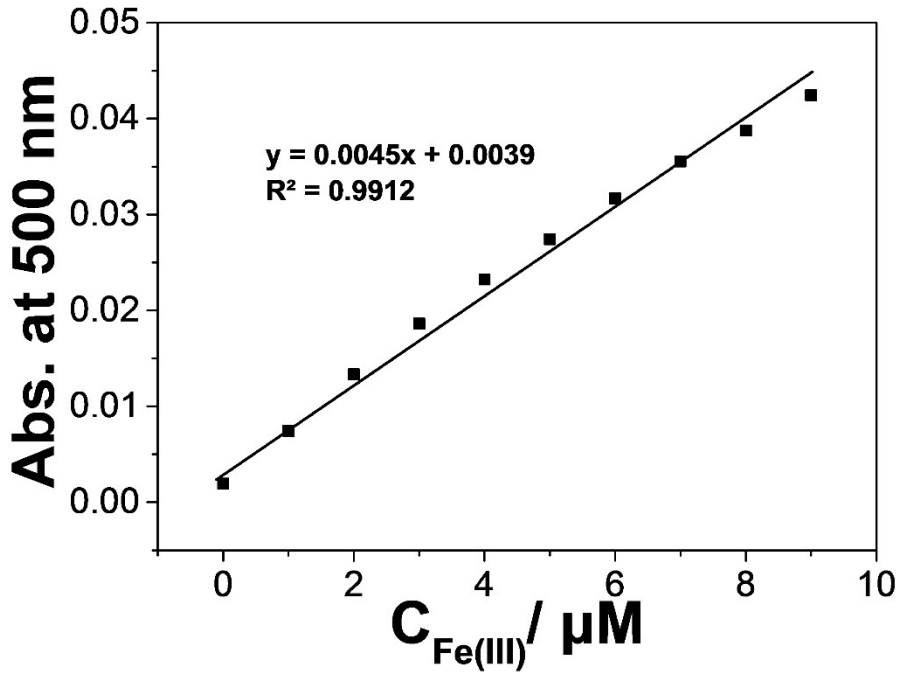

Fig. S30 UV-vis absorption intensity (at 500 nm) of **DHIC** as a function of Fe^{3+} concentration ([**DHIC**] = 20 μM and [Fe^{3+}] = 0.0-9.0 μM).